DETC2013-12582

EXTENSIBLE-LINK KINEMATIC MODEL FOR DETERMINING MOTION CHARACTERISTICS OF COMPLIANT MECHANISMS

Justin Beroz*[1,3], Shorya Awtar[2], A. John Hart[1,3]
[1]Mechanosynthesis Group, [2]Precision Systems Design Laboratory
Department of Mechanical Engineering, University of Michigan
Ann Arbor, MI 48109
[3]Department of Mechanical Engineering, Massachusetts Institute of Technology
Cambridge, MA 02139

ABSTRACT

We present an extensible-link kinematic model for characterizing the motion trajectory of an arbitrary planar compliant mechanism. This is accomplished by creating an analogous kinematic model consisting of links that change length over the course of actuation to represent elastic deformation of the compliant mechanism. Within the model, the motion trajectory is represented as an analytical function. By Taylor series expansion, the trajectory is expressed in a parametric formulation composed of load-independent and load-dependent terms. Here, the load-independent terms are entirely defined by the shape of the undeformed compliant mechanism topology, and all load-geometry interdependencies are captured by the load-dependent terms. This formulation adds insight to the process for designing compliant mechanisms for high accuracy motion applications because: (1) inspection of the load-independent terms enables determination of specific topology modifications for improving the accuracy of the motion trajectory; and (2) the load-dependent terms reveal the polynomial orders of principally uncorrectable error components of the motion trajectory. The error components in the trajectory simply represent the deviation of the actual motion trajectory provided by the compliant mechanism compared to the ideally desired one. We develop the generalized model framework, and then demonstrate its utility by designing a compliant micro-gripper with straight-line parallel jaw motion. We use the model to analytically determine all topology modifications for optimizing the jaw trajectory, and to predict the polynomial order of the uncorrectable trajectory components. The jaw trajectory is then optimized by iterative finite elements (FE) simulation until the polynomial order of the uncorrectable trajectory component becomes apparent.

1. INTRODUCTION

In high accuracy motion applications, the topology of a compliant mechanism is typically designed to provide a desired motion trajectory within a set of constraints, which may include the available mechanism area (i.e., the "footprint"), the means of actuation, the material properties, and the capabilities of the fabrication process. As shown schematically in Fig. 1, this topology must be designed to fit within the available mechanism area, be anchored at the available ground location(s), and comprise the "trajectory body", with respect to which the desired motion trajectory, $\Omega_d(\xi)$, is defined. The trajectory $\Omega_d(\xi)$ is the translation of a particular material point on the trajectory body, or the translation/rotation of the trajectory body, and is achieved by actuation of the compliant mechanism via the applied load. The desired trajectory is considered a function of the stroke parameter, ξ, which may represent either the applied load or the motion component of a body comprising the compliant mechanism that is critical to defining the desired trajectory. Here, ξ_0 corresponds to the undeformed state of the compliant mechanism.
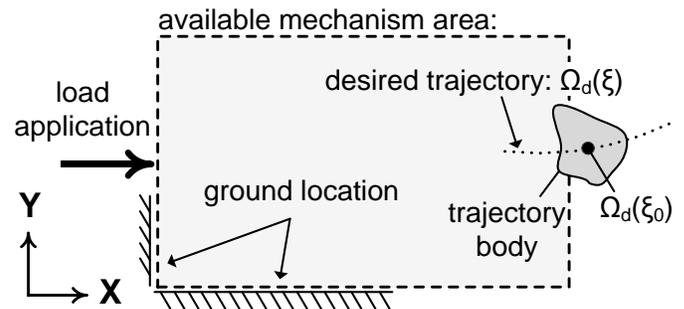

FIGURE 1: Representative compliant mechanism design scenario for high accuracy motion applications.

---

* Corresponding Author (jberoz@mit.edu)

An important part of the design process is to evaluate a candidate compliant mechanism topology by determining the accuracy with which it can trace the desired trajectory. Generally speaking, the motion trajectory of a compliant mechanism is dependent on the load application and on the mechanism topology. These dependencies are coupled, which adds difficulty to understanding and predicting the exact motion characteristics of a candidate mechanism topology. Topology symmetry is often utilized to avoid this complication, yet this is only feasible where there is adequate available mechanism area, and only for certain desired trajectories (i.e., straight-lines). If topology symmetry is not feasible given the shape of the desired trajectory and/or design domain limitations, evaluating the trajectory accuracy of a candidate compliant mechanism is nontrivial.

Several analytical methods have been developed that address this evaluation task. For instance, the Pseudo-Rigid-Body Model (PRBM) [1, 2] approximates the motion trajectory of a compliant mechanism by means of an analogous rigid-body mechanism. Alternatively, closed-form analytical solutions have been developed for compliant mechanisms built from beam flexures to capture kinematic, elastic, and elastokinematic effects [3, 4]. However, the shape and intricacy of the candidate compliant mechanism topology, and/or the nature of the applied load, may limit the accuracy by which these methods can evaluate its motion trajectory.

In such cases, finite elements (FE) modeling is the only well-established tool for evaluating the exact trajectory accuracy of a candidate compliant mechanism. Therefore, FE modeling is often utilized in conjunction with the aforementioned analytical models, as well as with recursive numerical procedures that integrate one or more the following design steps: (1) synthesis of a candidate compliant mechanism topology; (2) evaluation of the mechanism's trajectory accuracy; and (3) optimization by means of modifying the mechanism topology so as to minimize trajectory inaccuracy. Approaches include multi-criterion [5, 6], continuous material distribution [7, 8], and genetic [9, 10] numerical optimization algorithms. With sufficient FE simulation iteration, it is possible, in many cases, to modify a candidate compliant mechanism topology so that it exhibits sufficient trajectory accuracy. However, even after this topology optimization, a compliant mechanism may still exhibit a *residual* error regarding its ability to trace the desired motion trajectory.

Importantly, neither FE modeling nor the recursive optimization methods elicit an understanding regarding the existence, magnitude, or characteristic form of this residual error trajectory. Considerable time can be spent modifying the candidate mechanism topology in an attempt to redress this residual error trajectory, which may in fact be fundamentally uncorrectable due to some aspect of the mechanism topology.

We therefore present an analytical modeling approach that aids in understanding and evaluating the motion trajectory characteristics of an arbitrary planar compliant mechanism designed to accomplish a high accuracy motion task (Fig. 1).

Here, we create an analogous kinematic model that preserves the orientation and connection points between bodies comprising the compliant mechanism topology, and allows the kinematic links to change length over the course of mechanism actuation. The length change represents elastic deformation of the compliant mechanism. Within this framework, the mechanism's trajectory and link extensions are expressed as analytical functions of the stroke parameter, ξ. A Taylor series expansion of the trajectory is then performed with respect to ξ. This enables the trajectory to be represented by two parametrically separated motion components: *rigid-body* terms that contain only link lengths and orientations related to the undeformed state of the compliant mechanism topology; and *deformation* terms that, in addition, contain link extension components.

The significance of this parametric representation is that the rigid-body terms and the deformation terms represent load-independent and load-dependent components of the compliant mechanism's motion trajectory, respectively. Because the rigid-body terms are load-independent and are solely described by the undeformed state of compliant mechanism topology, they constitute a well-defined motion trajectory component that is entirely specifiable by design. Conversely, the deformation terms capture all load-geometry interdependencies, which necessarily arise over the course of mechanism actuation. Therefore, their magnitudes are dependent on the distribution of compliance throughout the mechanism topology. Within this framework, topology optimization may be regarded as a procedure in which the summation of the motion contributions from the rigid-body terms and deformation terms is designed to exhibit the desired trajectory.

This approach can streamline the compliant mechanism design process because: (1) inspection of the rigid-body terms enables specific topology modifications to be determined for minimizing the error trajectory; and (2) the polynomial orders of principally uncorrectable trajectory components are captured by the deformation terms. While optimization of the compliant mechanism trajectory must still be performed by iterative FE simulation, all geometric correction parameters for the mechanism topology, as well as the characteristic form of the residual error trajectory, are known beforehand. As a result, ineffective mechanism designs and topology modifications may be disregarded without FE simulation, and time is not spent attempting to redress trajectory errors that are principally uncorrectable via topology optimization. This serves to reduce the amount of time and number of numerical iterations necessary to arrive at a compliant mechanism topology that meets or exceeds the requirements for motion accuracy.

In the sections that follow, we present the analytical framework for an extensible-link kinematic model (ELKM) and describe how it may be utilized, in conjunction with FE modeling, as a design and optimization method (section 2). The utility of the method is then demonstrated in a case study (section 3), where we design a compliant gripping mechanism with a straight-line parallel jaw trajectory. The model is used to

determine the polynomial order of the residual jaw error trajectory, and to guide optimization of the jaw motion by iterative FE simulation.

2. GENERALIZED EXTENSIBLE-LINK MODEL

We begin with a candidate compliant mechanism having a desired motion trajectory, $\Omega_d(\xi)$, denoted in a global coordinate frame, which is considered a function of stroke parameter, ξ (Fig. 1). We define the actual motion trajectory of this corresponding point/body on the compliant mechanism by $\Omega_c(\xi)$, which is also a function of the same stroke parameter, ξ. Ideally, the this trajectory, $\Omega_c(\xi)$, and the desired trajectory, $\Omega_d(\xi)$, are equivalent. Therefore, the error trajectory, $\delta(\xi)$, is the difference $\Omega_c(\xi) - \Omega_d(\xi)$. Here, ξ_0 corresponds to the undeformed state of the compliant mechanism; and the deformed states of the mechanism within the range of actuation are defined by $\xi - \xi_0$. Because this actuation range is limited by material strain, $\Omega_d(\xi)$ and $\Omega_c(\xi)$ may each be reasonably represented by a smooth continuous function. However, in general, $\Omega_d(\xi)$ and $\Omega_c(\xi)$ may each comprise a set of piece-wise continuous functions in global coordinates, and the following analysis would be performed for each component of the set.
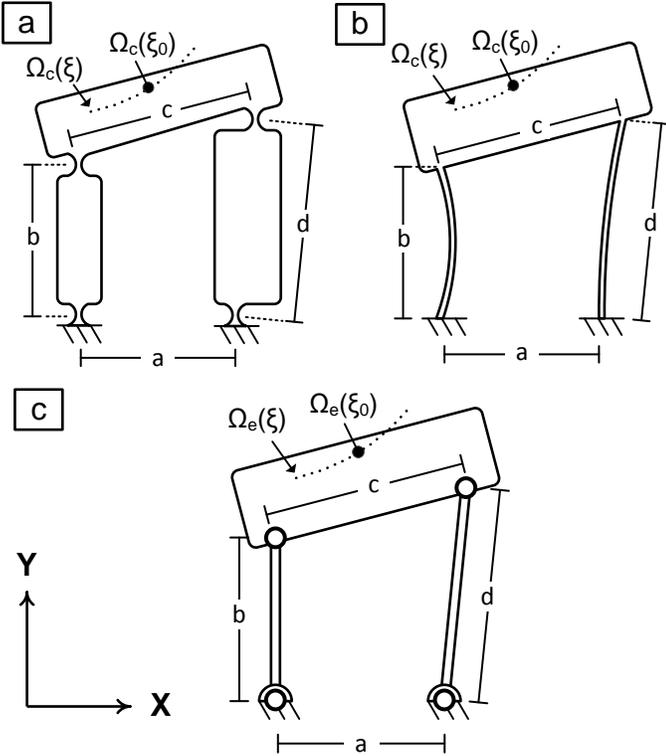

FIGURE 2: (a) Example lumped compliance and (b) distributed compliance compliant mechanisms (c) sharing the same kinematic model analogous to their undeformed topologies at ξ_0.

Next, an analogous kinematic model is created from the undeformed state of the compliant mechanism topology. Pin joint connections between kinematic links are placed at the same locations as the connection points between the bodies and

members comprising the compliant mechanism topology. The kinematic links are allowed to change length so that the pin joints track these points of connection in the compliant mechanism over the course of actuation. The length change of the links thereby represents elastic deformation of the compliant mechanism due to actuator loading. The fundamental concept underlying this model is that, regardless of compliance distribution, load application, or deformation during actuation, the points of connection between the bodies and members comprising the compliant mechanism topology are always preserved; and this necessarily constitutes some degree of kinematic constraint.

An extensible-link kinematic model (Fig. 2c) can be created from the undeformed state of any two-dimensional compliant mechanism topology, ranging from lumped compliance (Fig. 2a) to distributed compliance (Fig. 2b). The trajectory of the compliant mechanism, $\Omega_c(\xi)$, is represented by the motion of the corresponding point/link in the model by $\Omega_e(\xi)$, which again is a function of the same stroke parameter, ξ (Fig. 2c). These two trajectories, $\Omega_c(\xi)$ and $\Omega_e(\xi)$, are equivalent so long as the links in the model extend in the proper manner over the range of actuation, $\xi - \xi_0$.

Using classical kinematic analysis techniques, an expression for the trajectory, $\Omega_e(\xi)$, is derived in terms of the lengths and orientations of the extensible links. Without loss of generality, $\Omega_e(\xi)$ may be expressed by its Taylor-series expansion (Eq. 1) about the undeformed state of the mechanism ($\xi = \xi_0$). All coefficients in the expansion, k_n, are functions of the extensible link lengths and orientations. Because the range of actuation, $\xi - \xi_0$, is limited by material strain, it can be expected that the expansion may be truncated as an ith-order polynomial, where higher-order terms are negligible.

$$\Omega_e(\xi) = \sum_{n=0}^{\infty} \frac{\Omega^{(n)}(\xi_0)}{n!} (\xi - \xi_0)^n \cong \sum_{n=0}^{i} k_n (\xi - \xi_0)^n \qquad (1)$$

Each extensible link length in the model is now defined in the general form of Eq. 2a. Here, each link length, l, comprises a rigid-body length, l_0, corresponding to the undeformed state of the topology, ξ_0, as illustrated in Fig. 2; and an extensible component, $\boldsymbol{f(\xi)}$ (notated in bold). These extensible components, expressed as functions of ξ, represent the load-dependent geometric and elastic deformation of the compliant mechanism that arises during actuation. This imparts a requirement on all extensible components to be smooth continuous functions that are equal to zero at the undeformed state of the mechanism, ξ_0, (Eq. 2b).

$$l = l_0 + \boldsymbol{f(\xi)} \qquad\qquad \boldsymbol{f(\xi_0)} = 0 \qquad (2a,b)$$

By incorporation of Eq. 2, the k_n coefficients in Eq.1 become functions of ξ (Eq. 3). Without loss of generality, each k_n coefficient is represented by its respective Taylor series expansion about the undeformed state of the mechanism, ξ_0. Based on the magnitude of the extensible components, $\boldsymbol{f(\xi)}$, over the stroke, the Taylor series expansion for each k_n

coefficient may be truncated at the jth order, respect to $(\xi-\xi_0)$, such that the higher-order terms, $k_{n,m>j}$, are negligible.

$$\Omega_e(\xi) \cong \sum_{n=0}^{i} \left[k_n(\xi) \right] (\xi - \xi_0)^n$$

$$= \sum_{n=0}^{i} \left[\sum_{m=0}^{\infty} k_{n,m} (\xi - \xi_0)^m \right] (\xi - \xi_0)^n \quad (3)$$

$$\cong \sum_{n=0}^{i} \sum_{m=0}^{j-n} k_{n,m} (\xi - \xi_0)^{n+m}$$

$$= \Omega_{e,RB}(\xi) + \Omega_{e,D}(\xi)$$

$$\Omega_{e,RB}(\xi) \triangleq \sum_{n=0}^{i} k_{n,0} (\xi - \xi_0)^n$$

$$\Omega_{e,D}(\xi) \triangleq \sum_{n=0}^{i} \sum_{m=1}^{j-n} k_{n,m} (\xi - \xi_0)^{n+m}$$

As a result of Eq. 2b, the first term in each k_n Taylor series, $k_{n,0}$, contains only l_0 link lengths, and are therefore called *rigid-body* terms. The constitution of these rigid-body terms are unaffected by the extensible components, $f(\xi)$, and therefore collectively represent a motion trajectory component that is load-independent. Notably, these terms exactly constitute the rigid-body motion trajectory, in series-representation, of the kinematic mechanism comprising only l_0 link lengths (i.e., as if all $f(\xi) \equiv 0$); and this is denoted by $\Omega_{e,RB}(\xi)$ in Eq. 3.

All remaining terms in each k_n Taylor series, $k_{n,m>0}$ (Eq. 3), contain rigid-body link lengths, l_0, as well as derivatives of the extensible components up to the mth-order, evaluated at ξ_0 (i.e., $f(\xi_0)^{(m)}$). These are called *deformation* terms, and their constitution is of a form such that they require the existence of extensible components, $f(\xi)$, to be non-zero valued; and their magnitude directly corresponds to the magnitude of the extensible component derivatives (i.e., $f(\xi_0)^{(m)}$). Hence, the values of the deformation terms: (1) capture the load-geometry interdependencies arising over the course of mechanism actuation; and (2) reflect the amount and distribution of compliance in the compliant mechanism topology.

$$\Omega_e(\Delta\xi) \cong \left[k_{0,0} \right] + \left[k_{1,0} + \boldsymbol{k_{0,1}} \right] \Delta\xi + \left[k_{2,0} + \boldsymbol{k_{1,1}} + \boldsymbol{k_{0,2}} \right] \Delta\xi^2$$

$$+ ... + \left[k_{i,0} + \sum_{n=0}^{i-1} \boldsymbol{k_{n,i-n}} \right] \Delta\xi^i + \left[\sum_{n=0}^{i} \boldsymbol{k_{n,i+1-n}} \right] \Delta\xi^{i+1} \quad (4)$$

$$+ ... + \left[\sum_{n=0}^{i} \boldsymbol{k_{n,j-n}} \right] \Delta\xi^j$$

$$\xi \triangleq \xi_0 + \Delta\xi$$

We now write the entire series expansion explicitly, grouping like-ordered $k_{n,m}$ terms (Eq. 4). For clarity, these terms are expressed as functions of $\Delta\xi$, which represents the displacement from the mechanism's undeformed state. The rigid-body, $k_{n,0}$, and deformation, $\boldsymbol{k_{n,m>0}}$ (notated in bold), terms

are now represented in a parametric form showing that there is one rigid-body term per polynomial order, terminating at the ith order with respect to $\Delta\xi$. Deformation terms may range from 1st order to j^{th} order, for some $j>i$.

Similarly, the desired motion trajectory, $\Omega_d(\xi)$, may be represented by its Taylor series expansion (Eq. 5), about the undeformed state of the mechanism, ξ_0.

$$\Omega_d(\Delta\xi) = \sum_{n=0}^{\infty} d_n (\Delta\xi)^n = d_0 + d_1\Delta\xi + d_2\Delta\xi^2 + ... \quad (5)$$

The summation of rigid-body and deformation terms per polynomial order (Eq. 4) is ideally equivalent to that of the desired trajectory (Eq. 5). By $\Omega_c(\xi) = \Omega_e(\xi)$, the error trajectory, $\delta(\xi)$, may be written as the difference $\Omega_e(\xi) - \Omega_d(\xi)$ (Eq. 6).

$$\delta(\Delta\xi) = \Omega_e(\Delta\xi) - \Omega_d(\Delta\xi)$$

$$= \left[k_{0,0} - d_0 \right] + \left[(k_{1,0} + \boldsymbol{k_{0,1}}) - d_1 \right] \Delta\xi$$

$$+ \left[(k_{2,0} + \boldsymbol{k_{1,1}} + \boldsymbol{k_{0,2}}) - d_2 \right] \Delta\xi^2$$

$$+ ... + \left[\left(k_{i,0} + \sum_{n=0}^{i-1} \boldsymbol{k_{n,i-n}} \right) - d_i \right] \Delta\xi^i \quad (6)$$

$$+ \left[\left(\sum_{n=0}^{i} \boldsymbol{k_{n,i+1-n}} \right) - d_{i+1} \right] \Delta\xi^{i+1}$$

$$+ ... + \left[\left(\sum_{n=0}^{i} \boldsymbol{k_{n,j-n}} \right) - d_j \right] \Delta\xi^j$$

Importantly, the deformation terms for any compliant mechanism topology will be nonzero; their *magnitudes* may only be minimized by a lumped-compliance topology or maximized by a distributed-compliance topology. Further, the minimum and maximum limits of compliance distribution are typically bounded by practical considerations such as: (1) the material yield strain, given the range of mechanism actuation, $\xi - \xi_0$; (2) the available mechanism area (Fig. 1); and (3) fabrication precision. In contrast, the *magnitudes and signs* of the rigid-body terms are entirely determined by the locations of connections (i.e., kinematic constraint) between the bodies and members comprising the compliant mechanism topology in its undeformed state, ξ_0; and these locations can be altered within the available mechanism area (Fig. 1) by design. Hence from a design perspective, the values of the rigid-body terms may be considered "completely specifiable by design", while the values of the deformation terms may be considered "partially specifiable by design".

By this insight, the procedure for minimizing the trajectory error (Eq. 6) of a compliant mechanism via topology optimization may be regarded as follows: per polynomial order, the value of each rigid-body term is designed to compensate for the corresponding deformation terms so as to provide the correct overall motion trajectory of that order. In other words, the kinematic constraint in the compliant mechanism topology is designed to compensate for load-dependent trajectory components that arise during actuation. Within this context, Eq.

6 illustrates that the error trajectory only up to the ith order may be, in total or in part, redressed by topology optimization. All trajectory components greater than or equal to the $(i+1)^{th}$ order are exclusively deformation terms, and are therefore, in principle, uncorrectable (i.e., only minimizable). By the nature of Taylor series expansions, it is likely that the $(i+1)$-order contribution will dominate any higher-order deformation terms.

Given a specific candidate compliant mechanism topology, the effectiveness of redressing the error trajectory via topology optimization can be determined by inspection of the rigid-body terms. The formulation for each $k_{n,0}$ term indicates how its value may be modified by changing the rigid-link lengths/orientations (i.e., l_0 in Eq. 2a), which thereby indicates how analogous topology changes in the compliant mechanism affect its trajectory. Ideally, there would be i-number of unique geometric parameters available, each of which could be independently changed to modify the value of corresponding $k_{n,0}$ terms. In this case, the residual trajectory error would consist of significant $(i+1)^{th}$ to j^{th} order polynomial components. Having less than i-number of suitable geometric modifications would constitute an over constraint in the optimization procedure, where an appropriate tradeoff would be determined between the values of two or more $k_{n,0}$ terms in order to minimize the error trajectory.

This model is useful for understanding the qualitative motion characteristics of compliant mechanisms and for guiding the design process. Notably, developing this model framework required no assumptions or constraints regarding the compliant mechanism topology, material properties, or compliance distribution within the topology. These specifications are all contained within the extensible components, $f(\xi)$, which can be, in principle, expressed in an analytical closed-form; and this would entail a synthesis of parametric numerical solutions for the appropriate elastically extensible compliant geometries. Although, the real utility of this model is in *not* having to specify explicit equations for the extensible components, which makes it amenable to analysis of mechanism topologies that cannot be represented in an analytical closed-form. For such cases, FE simulation can be used in conjunction with the model in an iterative procedure to minimize the trajectory error by topology optimization. The procedure is summarized below, and depicted in Fig. 3. Note that it is analytical until the last step, where iterative numerical simulation is used to minimize the error trajectory (Fig. 3, dashed box).

1. First, the formulations of the rigid-body terms constituting the trajectory $\Omega_{e,RB}(\xi)$ are determined by kinematic analysis. The kinematic model (Fig. 2c) is derived based on the locations of connection between the bodies and members that comprise the compliant mechanism at its undeformed state, ξ_0.
2. The rigid-body terms are then analyzed to determine the geometric correction parameters. These parameters will correspond to the orientations and/or l_0 lengths of particular links at the undeformed state of the mechanism, ξ_0. The optimization procedure will be over-constrained if fewer than i-number of independent geometric parameters exist

(Eq. 6); and the designer may make a judgment call on whether to proceed to optimizing the current topology candidate, or to synthesize a new topology, resulting in a new extensible-link kinematic model. This step also enables the polynomial order of the residual error trajectory to be predicted (i.e., the error trajectory remaining after topology optimization).

3. Next, the error trajectory is minimized via topology optimization, where FE simulation is used to quantify the exact trajectory, $\Omega_e(\xi)$. Since the values of the rigid-body terms, $k_{n,0}$, are known analytically, fitting a jth-order polynomial curve to the FE simulated trajectory quantifies the net motion contribution of the deformation term(s) per polynomial order.
4. The magnitude and sign of these net deformation term contributions inform the designer on how to modify each geometric correction parameter for the next FE simulation.
5. This iteration may continue until: (1) the magnitude of the error trajectory is reduced below the design specifications; or (2) the polynomial order of the residual error trajectory becomes apparent, since this signifies the limit of correction via topology optimization for the candidate compliant mechanism topology.
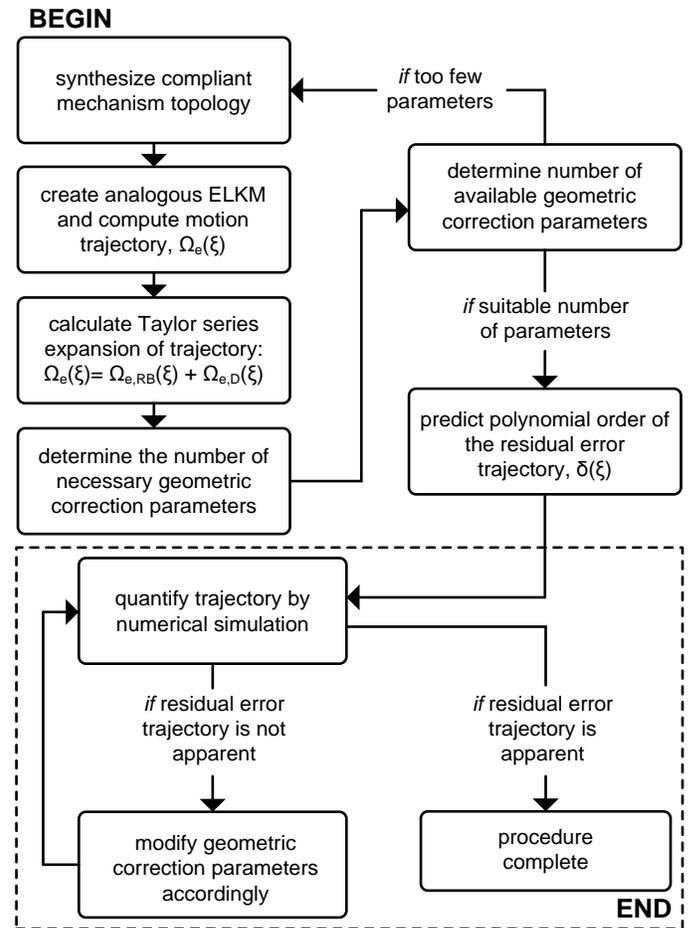

FIGURE 3: Compliant mechanism design procedure utilizing the Extensible-link Kinematic Model (ELKM).

3. DESIGN OF A MICRORGIPPER WITH STRAIGHT-LINE JAW TRAJECTORY

We demonstrate the utility and validity of the extensible link kinematic model by designing a compliant gripping mechanism with a straight-line parallel jaw trajectory. Straight-line jaw motion may be desired for micromechanical tension/compression tests, and for gripping soft objects such as cells, gels, and assemblies of micro and nanostructures. These and other applications are sensitive to normal and shear forces, and therefore it is important to decouple these two loading conditions.
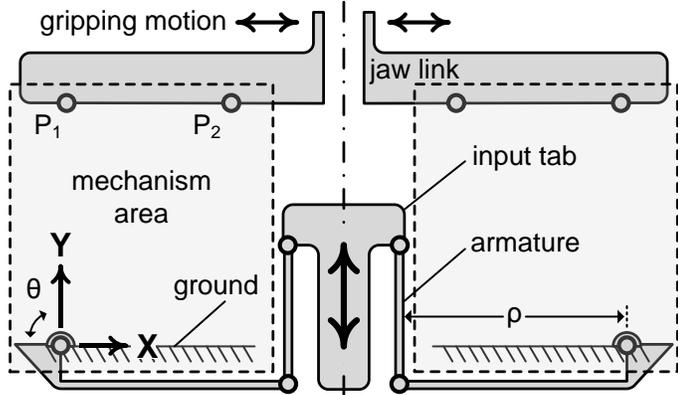

FIGURE 4: Displacement-constraint design problem for parallel-jaw gripping mechanism, where mirror-image topologies fill right and left mechanism areas.

For this task, we require a compliant mechanism topology within the indicated available area (Fig. 4, dashed box). This mechanism ideally enables pure X-direction rigid-body translation of the gripper jaw links without rotation. Translation of the jaw link in the Y-direction, as well as jaw link rotation, constitute error trajectories. For use of this gripper in micromanipulation tasks, we desire a 400μm jaw actuation range (i.e., ±100μm X-displacement per jaw link), over which the Y-displacement of the jaw trajectory is less than 10nm.

In order to achieve mirrored precision motion of both gripper faces, a single input motion provided by one actuator drives the actuation of both gripper jaws. This is enabled by the armature configuration (Fig. 4), which serves to translate linear motion of the input tab, provided by the actuator, to rotary motion, θ, about a grounded pivot. By design, the gripper jaw displacement may be proportional to the input tab displacement by means of small angle approximation with respect to θ (Eq. 7). This proportional relationship may be tuned based on armature length, ρ, which makes this configuration, and variants thereof, suitable for either amplifying the displacement of piezoelectric actuators or deamplifying the motion of traditional linear actuators. The design task is therefore to determine a compliant mechanism topology that fits within the mechanism area, anchors at the available ground, and converts rotation of the grounded armature pivot, θ, to horizontal translation of the gripper jaws.

$$\theta = \theta_0 + \Delta\theta, \qquad |\Delta\theta| \leq 2^o \qquad (7)$$

The location of the mechanism area (Fig. 4) is driven by two main considerations: (1) it is desirable to minimize the overall mechanism size; and (2) the mechanism area may not extend vertically above the jaw link, otherwise sample manipulation and viewing are obstructed. Note that this second consideration rules out the possibility of utilizing symmetry in the mechanism topology to achieve straight line motion.

The motion paths of points P_1 and P_2 (Fig. 4) define the rigid-body trajectory of the jaw link. We regard the rigid-body translation of the jaw link to be equivalent to the trajectory of P_1, and jaw link rotation to be attributable to inaccurate duplication of the P_1 motion at P_2. Ideally, P_1 translates horizontally and this motion is perfectly duplicated at P_2. Separating rigid-body translation and rotation in this manner greatly simplifies the following analysis of the accuracy limits of gripper jaw trajectory.
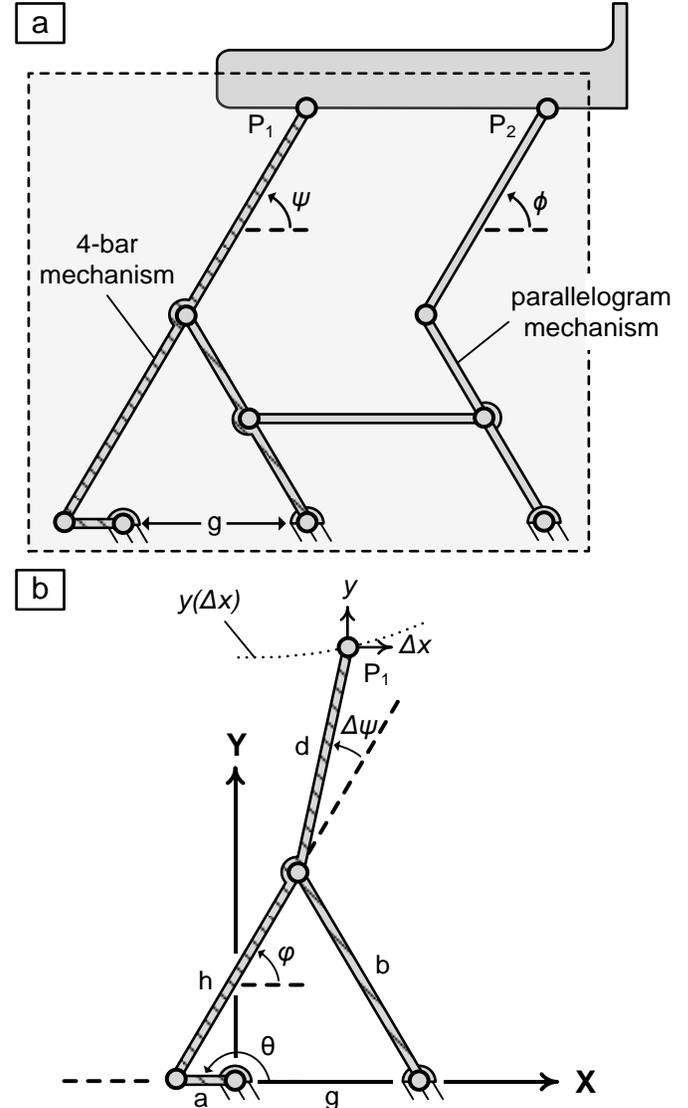

FIGURE 5: (a) Mechanism solution for straight-line horizontal jaw displacement, which utilizes (b) a 4-bar mechanism based on the Hoekens linkage to determine the motion of P_1.

We now consider an extensible-link kinematic model in the mechanism area (Fig. 5) that consists of: a closed 4-bar mechanism (hashed shading) that defines the path of P_1, and a parallelogram-based mechanism that serves to duplicate the motion of P_1 at P_2. Referencing the classical Hoekens linkage as a starting point, we define the geometric parameters of the 4-bar as follows (Fig. 5b): a = crank, g = ground, b = follower, h = output, d = extension of h to P_1 at relative angle ψ. We write the vector trajectory of P_1 in the global X-Y coordinate system (Eq. 8) such that it comprises only the input crank angle, θ, defined with respect to the X-axis as shown, and the kinematic linkage arrangement (i.e., extensible link lengths and angle ψ). The expression for the internal angle, φ, is derived based on the kinematic constraint that the ends of link h must coincide with the respective ends of links a and b.

$$\mathbf{P_1} = \begin{bmatrix} x \\ y \end{bmatrix} = a \begin{bmatrix} \cos\theta \\ \sin\theta \end{bmatrix} + h \begin{bmatrix} \cos\varphi \\ \sin\varphi \end{bmatrix} + d \begin{bmatrix} \cos(\varphi+\psi) \\ \sin(\varphi+\psi) \end{bmatrix} \quad (8)$$

$$\varphi \triangleq \arcsin\left(\frac{b^2 - a^2 - h^2 - g^2 + 2ag\cos\theta}{\sqrt{(2ah\sin\theta)^2 + (2h(a\cos\theta - g))^2}} \right)$$
$$- \arctan\left(\frac{a\cos\theta - g}{a\sin\theta} \right)$$

By kinematic analysis, this P_1 trajectory may expressed as the function, $y(\Delta x)$, in the global X-Y coordinate system, where its 2nd-order Taylor-series expansion (i.e., $i=2$ in Eq. 3) is sufficient to capture all significant motion contributions for small angular perturbations, $\Delta\theta$ (Eq. 7). Here, the y-direction motion is represented as a function of the gripping direction displacement, Δx (i.e., the stroke parameter). Note that the desired trajectory is: $y(\Delta x)$=constant (i.e., horizontal translation of P_1).

$$y(\Delta x) \cong k_0 + k_1 \Delta x + k_2 \Delta x^2 \quad (9)$$

Each extensible beam is now given the definitional form $l = l_0 + f(\Delta x)$ (Eq. 2), where l_0 is the rigid-link length and the extensible component, $f(\Delta x)$, is a smooth non-constant function satisfying $f(0)=0$. This makes each k_n term (Eq. 9) a function of Δx. By Taylor series expansion of these k_n terms about $\Delta x=0$ for $j=3$ (referencing Eq. 3), and collection of like-ordered terms, we arrive at Eq. 10. Here, it is clear that the 3rd order trajectory component is, in principle, uncorrectable because it contains only deformation terms (notated in bold). We see that it is sufficient to truncate the series representation at $j=3$ because all higher-order terms are exclusively deformation terms, and will be dominated by this 3rd order contribution over the stroke range (i.e., $\Delta x = \pm 100 \mu m$). The rigid-body terms, $k_{n,0}$, are derived and shown explicitly because they will be analyzed to determine the geometric correction parameters for optimization of the compliant mechanism topology.

$$y(\Delta x) \cong k_{0,0} + \left[k_{1,0} + \mathbf{k_{0,1}} \right] \Delta x$$
$$+ \left[k_{2,0} + \mathbf{k_{1,1}} + \mathbf{k_{0,2}} \right] \Delta x^2 \quad (10)$$
$$+ \left[\mathbf{k_{2,1}} + \mathbf{k_{1,2}} + \mathbf{k_{0,3}} \right] \Delta x^3$$

$$k_{0,0} = \sqrt{1 - R_0^2} \left(h_0 + d_0 \cos\psi \right) + R_0 d_0 \sin\psi \quad (11a)$$

$$k_{1,0} = \frac{a_0 + g_0 - R_0 \left(h_0 + d_0 \cos\psi \right) + d_0 \sqrt{1 - R_0^2} \sin\psi}{\sqrt{1 - R_0^2} \left(h_0 + d_0 \cos\psi \right) + R_0 d_0 \sin\psi} \quad (11b)$$

$$k_{2,0} = \left\{ \left(\frac{R_0^2 h_0 (a_0 - g_0) + R_0 g_0 (a_0 + g_0) - h_0 a_0}{2 h_0 a_0} \right) \right.$$
$$\times \frac{h_0 + d_0 \cos\psi}{\sqrt{1 - R_0^2}}$$
$$\left. - \left(\frac{R_0 h_0 (a_0 - g_0) + g_0 (a_0 + g_0)}{2 h_0 a_0} \right) d_0 \sin\psi \right\} \quad (11c)$$
$$\div \left(\sqrt{1 - R_0^2} \left(h_0 + d_0 \cos\psi \right) + R_0 d_0 \sin\psi \right)^2$$

$$R_0 \triangleq \frac{a_0^2 + h_0^2 + g_0^2 - b_0^2 + 2a_0 g_0}{2 h_0 (a_0 + g_0)}$$

For brevity, the $k_{n,0}$ expressions (Eq. 11) include the substitution $\theta_0 = 180^0$, which we determined, by inspection, to be requisite for a symmetric P_1 trajectory about the undeformed state of the mechanism. Here, symmetric trajectories occur for the following kinematic relationships: $\psi = 0^0$, $h_0=b_0=d_0$, considering equal angular perturbations of the crank (i.e., link a) about θ_0. By analysis of the $k_{n,0}$ terms (Eq. 11), we determined that perfect horizontal straight-line motion (i.e., $k_{1,0} = k_{2,0} = 0$) is achieved for the following kinematic relationship: $h_0=b_0=d_0=l_0$, such that $l_0/a_0 = 4$ and $g_0 = l_0-a_0$. These link length relationships are slightly different than that of the classical Hoekens mechanism (i.e., $l_0/a_0 = 2.5$). To achieve the desired jaw range (0-400μm) given the small-angle restriction (Eq. 7), $a_0 = 1.67mm$ is required, which is practically feasible.

By analysis of the rigid-body terms (Eq. 11), we find that both the sign and magnitude of $k_{1,0}$ and $k_{2,0}$ may be controlled by independently changing ψ and g_0, respectively (Fig. 6). Therefore, the 1st and 2nd order trajectory errors caused by the corresponding-order deformation terms may be completely corrected by optimization of these two geometric parameters. Hence, we can predict the residual error trajectory of the gripper jaw after optimization to be a 3rd-order polynomial that is, in principle, not correctable. Note that, even though the 3rd-order rigid-body term (i.e., $k_{3,0}$) is negligible, the cumulative contribution from the 3rd-order deformation terms (i.e.,

$k_{2,1}+k_{1,2}+k_{0,3}$) may be significant in magnitude. In order to eliminate this 3rd-order error, a different mechanism topology would have to be considered, having a significant $k_{3,0}$ term with three unique geometric parameters that could be independently modified to change the values of $k_{1,0}$, $k_{2,0}$, and $k_{3,0}$.
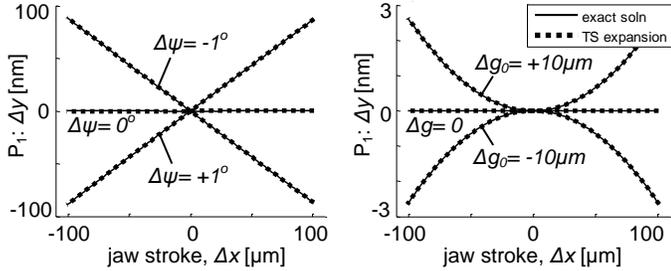

FIGURE 6: *Modification of geometric parameters $\Delta\psi$ and Δg_0 are utilized to correct 1st and 2nd order P_1 trajectory errors, respectively.*

So far, only the trajectory of P_1 has been considered. To achieve the desired gripper jaw motion, the P_1 trajectory must be duplicated at P_2 by the parallelogram linkage portion of the mechanism (Fig. 5a). The above parametric analysis may be performed for this parallelogram linkage as well in order to express the motion of P_2 in a parametric form. But, for brevity and clarity, we simply note that all significant contributions to the trajectory of P_2 may be captured in the form on Eq. 10 because all links in the parallelogram linkage are subject to the small angle constraint (Eq. 7). By analogy, we conclude that adjusting ϕ (Fig. 5a) modifies the linear trajectory of P_2. This angle will be optimized in order to minimize gripper jaw rotation, ω; and as our FE results will show, this linear correction of the P_2 trajectory is sufficient.
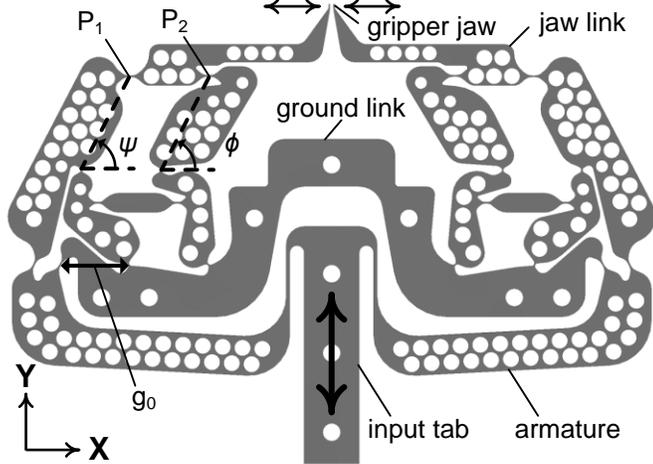

FIGURE 7: *Lumped-compliance gripper topology with straight-line parallel-jaw trajectory based on the Hoekens 4-bar linkage.*

The Hoekens-based kinematic mechanism (Fig. 5a) is translated into a lumped-compliance flexure mechanism (Fig. 7, [12]) now that all suitable topology modifications have been determined. Here, the geometric centers of thin compliant hinges (Fig. 7) coincide with the locations of the pin joints in

the kinematic model (Fig. 5a). The hinges have a cycloidal profile [11] which, compared to other compliant hinge contours, maximizes in-plane rotational compliance and translational stiffness for a prescribed angular deflection limit (Eq. 7) and allowable material strain. For microfabrication of the gripper from a silicon wafer, we choose a strain limit of 0.5% [13]. Note that a lumped-compliance topology has been chosen in order to minimize the magnitude of the deformation terms, $k_{n,m>0}$, and thereby the magnitude of the residual error trajectory.
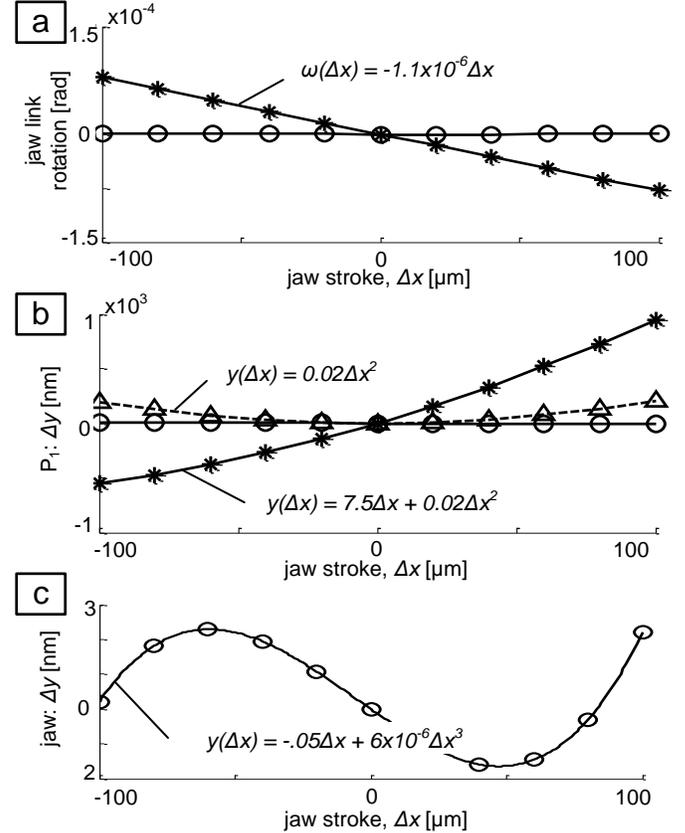

FIGURE 8: *Demonstration of reduced jaw trajectory error in (a) jaw link rotation over the jaw stroke, Δx, between initial (*) and optimized (o) FE simulations; and (b) P_1 trajectory over jaw stroke between initial (*), 1st-order optimized only (Δ), and fully optimized (o) FE simulations. (c) The optimized jaw trajectory exhibits a residual 3rd-order error, as predicted.*

The compliant mechanism topology is now optimized by iterative manual adjustment and evaluation by nonlinear FE simulation in ANSYS. The rotation (Fig. 8a) and translation (Fig. 8b) of the jaw over the stroke, Δx, are plotted for the initial (*) and final (o) FE simulations. The topology for the initial simulation has model link lengths corresponding to $k_{1,0} = k_{2,0} = 0$, and therefore the error trajectory here is entirely attributable to the deformation terms, $k_{n,m>0}$, in the kinematic model. The polynomial curves fitted to the jaw rotation, $\omega(\Delta x)$, and P_1 trajectory, $y(\Delta x)$, quantify the net deformation-term motion contribution per polynomial order, which informs the designer on how to modify the geometric parameters (i.e., $\Delta\psi, \Delta g_0, \Delta\phi$)

to minimize the error trajectory. The results from the initial FE simulation (Fig. 8a,b, asterisks) indicate the following modifications: increase ϕ with respect to ψ to redress jaw rotation [5]; decrease ψ and g_0 to redress jaw translation errors (Fig. 6). All three geometric parameters may be modified at once.

The influence of these modifications is evaluated by subsequent FE simulation, and iteration continues until the polynomial order of the predicted residual error trajectory becomes apparent. To illustrate the validity of this model, we also show an intermediate step where we only correct the linear trajectory component of P_1 (i.e., $\Delta\psi$), resulting in a parabolic error trajectory (Fig. 8b, triangles). It is to be noted that the deformation terms, $k_{n,m>0}$, include rigid link lengths (i.e., l_0 in Eq. 2a) as well as extensible components, $f(\xi)$, and therefore their magnitudes are partially dependent on the undeformed state of the topology. This implies that the optimization procedure here is inherently iterative because modifying the topology changes the value of the rigid-body terms and the deformation terms.

Fewer than 30 iterations were required to reach the optimized topology, and the final geometric modifications with respect to the initial topology, as denoted in Fig. 7, were: $\Delta\psi = -0.850^o$, $\Delta g_0 = -0.7mm$, $\Delta\phi = -0.354^o$. The final compliant gripper has jaw rotation less than 0.8μrad and translation error less than 5nm over the entire stroke according to the final FE simulation (Fig. 8a,b,c; circles). The residual error trajectory of the gripper jaw is 3rd-order, as predicted (Fig. 8c). This is the limit of trajectory error correction via topology optimization for the compliant mechanism (Fig. 7).

4. CONCLUSION

We have developed an extensible-link kinematic model for understanding the motion characteristics of compliant mechanisms using a parametric formulation. Within this framework, the trajectory of a compliant mechanism consists of distinct motion components that are either: (1) load-independent and entirely specifiable by the mechanism topology (i.e., *rigid body* terms); or (2) load-dependent and represent all load-geometry interdependencies that arise during mechanism actuation (i.e., *deformation* terms). This elucidates insights about the fundamental sources of trajectory error in a compliant mechanism topology, and therefore the limits with which it can be corrected by topology optimization. A compliant microgripper (Fig. 7) is designed, which demonstrates the utility of this model for streamlining the compliant mechanism design and topology optimization processes, in conjunction FE simulation. The model is particularly useful for non-symmetric mechanism topologies that are too complex to represent in an analytical closed form.

5. ACKNOWLEDGMENTS

REFERENCES
1. Howell, L. L., and Midha, A., 1994, "A Method for the Design of Compliant Mechanisms with Small-length Flexural Pivots," Journal of Mechanical Design, 116(1), pp. 280-290.
2. Howell, L. L., and Midha, A., 1995, "Parametric Deflection Approximations for End-loaded Large-deflection Beams in Compliant Mechanisms," Journal of Mechanical Design, 117(1), pp. 156-165.
3. Awtar, S., and Slocum, A. H., 2007, "Constraint-based design of parallel kinematic XY flexure mechanisms," Journal of Mechanical Design, 129(8), pp. 816-830.
4. Awtar, S., Slocum, A. H., and Sevincer, E., 2007, "Characteristics of beam-based flexure modules," Journal of Mechanical Design, 129(6), pp. 625-639.
5. Frecker, M. I., Ananthasuresh, G. K., Nishiwaki, S., Kikuchi, N., and Kota, S., 1997, "Topological synthesis of compliant mechanisms using multi-criteria optimization," Journal of Mechanical Design, 119(2), pp. 238-245.
6. Saxena, A., and Ananthasuresh, G. K., 2000, "On an optimal property of compliant topologies," Structural and Multidisciplinary Optimization, 19(1), pp. 36-49.
7. Carbonari, R. C., Silva, E. C. N., and Nishiwaki, S., 2005, "Design of piezoelectric multi-actuated microtools using topology optimization," Smart Materials & Structures, 14(6), pp. 1431-1447.
8. Matsui, K., and Terada, K., 2004, "Continuous approximation of material distribution for topology optimization," International Journal for Numerical Methods in Engineering, 59(14), pp. 1925-1944.
9. Tai, K., and Chee, T. H., 2000, "Design of structures and compliant mechanisms by evolutionary optimization of morphological representations of topology," Journal of Mechanical Design, 122(4), pp. 560-566.
10. Lu, K. J., and Kota, S., 2006, "Topology and dimensional synthesis of compliant mechanisms using discrete optimization," Journal of Mechanical Design, 128(5), pp. 1080-1091.
11. Tian, Y., Shirinzadeh, B., Zhang, D., and Zhong, Y., 2010, "Three flexure hinges for compliant mechanism designs based on dimensionless graph analysis," Precision Engineering-Journal of the International Societies for Precision Engineering and Nanotechnology, 34(1), pp. 92-100.
12. Beroz, J., Awtar, S., Bedewy, M., Sameh, T., Hart, A.J., 2011, "Compliant Microgripper with Parallel Straight-line Jaw Trajectory for Nanostructure Manipulation," Proceedings of 26th American Society of Precision Engineering Annual Meeting, Denver, CO.
13. Ando, T., Sato, K., Shikida, M., Yoshioka, T., Yoshikawa, Y., Kawabata, T., and Ieee, I., 1997, "Orientation-dependent fracture strain in single-crystal silicon beams under uniaxial tensile conditions," Mhs'97: Proceedings of 1997 International Symposium on Micromechatronics and Human Science